Soft Matter

PAPER

View Article Online
View Journal | View Issue

Cite this: *Soft Matter*, 2015, **11**, 1701

Self-assembled nanoparticle micro-shells templated by liquid crystal sorting†

Andrea L. Rodarte,[a] Blessing H. Cao,[b] Harmanpreet Panesar,[b] Ronald J. Pandolfi,[a] Makiko Quint,[a] Lauren Edwards,[a] Sayantani Ghosh,[a] Jason E. Hein*[b] and Linda S. Hirst*[a]

Received 23rd October 2014
Accepted 11th December 2014

DOI: 10.1039/c4sm02326a

www.rsc.org/softmatter

A current goal in nanotechnology focuses on the assembly of different nanoparticle types into 3D organized structures. In this paper we report the use of a liquid crystal host phase in a new process for the generation of micron-scale vesicle-like nanoparticle shells stabilized by ligand–ligand interactions. The constructs formed consist of a robust, thin spherical layer, composed of closely packed quantum dots (QDs) and stabilized by local crystallization of the mesogenic ligands. Ligand structure can be tuned to vary QD packing within the shell and made UV cross-linkable to allow for intact shell extraction into toluene. The assembly method we describe could be extended to other nanoparticle types (metallic, magnetic *etc.*), where hollow shell formation is controlled by thermally sorting mesogen-functionalized nanoparticles in a liquid crystalline host material at the isotropic to nematic transition. This process represents a versatile method for making non-planar 3D nano-assemblies.

Introduction

A current challenge in nano-science is to address the problem of organizing nanoparticles of different types into well-ordered 2D and 3D assemblies on a macroscopic scale. The recently emerged hierarchical NP super-lattices or cluster assemblies, often referred to as "meta-materials", have been shown to exhibit exciting new collective electronic, photonic or magnetic properties[1,2] distinct from those of individual particles or bulk material. In general, there are two different approaches to fabricating ordered arrays of NPs: top-down nanofabrication (*i.e.* lithographic techniques) or bottom-up self- or directed-assembly methods. A critical drawback to existing methods has been in spatial scale and the ability to produce non-planar 3D architectures.

Nano-crystal assemblies are examples of cluster-assembled materials.[3] If their size is tightly controlled, solution based assembly methods can be generalized to include a vast array of particle combinations as seen on a smaller scales so far in 2D and 3D assemblies.[4–6] Recent attempts at assemblies of gold particle clusters[7] have used a variety of particle spacing methods including biopolymers,[8,9] proteins[10,11] and block copolymers.[12–14]

Given that a solution-based approach provides the best chance for large-scale manufacturing, our work focuses on a fluid-based approach to NP assembly. In this paper, we report a liquid crystal droplet templated process that takes advantage of the phase dependent miscibility of mesogen-functionalized quantum dots (QDs) in a nematic liquid crystal to produce micron-scale vesicles or spherical 'shells' of QDs. The shells are mechanically robust, stable up to temperatures of ~110 °C, and can be extracted intact from the host LC phase. Addition of a UV cross-linkable ligand further enhances shell stability following formation, demonstrating the applicability of these structures to a wide variety of photonic and materials applications.

Liquid crystals are anisotropic fluids in which the constituent molecules have local orientational order along an axis defined by the director, ***c***. The temperature range of liquid crystal phases exhibited by a material can be fine-tuned by careful control of molecular structure or by mixing the material with different LC or non-LC molecules, producing a variety of LC phases. Common liquid crystal phases include the nematic phase – well known for its use in display technologies, and the layered smectic phase.

For this study we designed and synthesized a series of ligands, exchanged onto the surface of CdSe/ZnS core–shell QDs. The chosen ligands are liquid crystalline or "mesogenic", and incorporate a rigid rod-like segment, with flexible attachment arms (Fig. 1). Mesogenic ligands have been used previously to aid the uniform dispersion of metallic NPs[15,16] in different LC materials. We recently reported the use of such

[a]*Department of Physics, University of California, Merced, 5200 Lake Rd, Merced, CA95343, USA. E-mail: lhirst@ucmerced.edu*

[b]*Department of Chemistry and Chemical Biology, University of California, Merced, 5200 Lake Rd, Merced, CA95343, USA. E-mail: Jhein2@ucmerced.edu*

† Electronic supplementary information (ESI) available: Complete descriptions of synthesis methods and sample characterization methods. Two fluorescence microscopy movies clearly demonstrate the shell formation process. See DOI: 10.1039/c4sm02326a

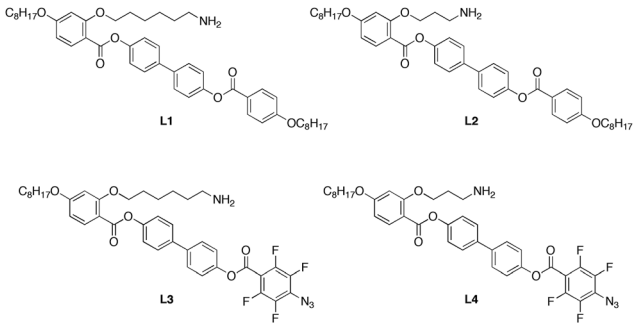

Fig. 1 Molecular structures for mesogenic ligands used in this paper.

ligands to disperse QDs in the nematic phase.[17] In these cases the ligand is designed to both be miscible with the host phase, and also to have the ability to rotate on a flexible arm and align with nematic phase surrounding the NP. Mesogenic ligands attached to a NP surface will tend to align with the director of a surrounding LC phase, provided the ligand core has enough rotational freedom and similar constructs have been shown to organize a tactoidal ligand distribution in an aligned nematic host phase.[18] Mesogen functionalized gold nanoparticles have also been shown to produce a rich intrinsic phase behavior.[19–21]

Liquid crystal mixtures are commonly used to tailor material properties for a specific application. If we mix two mesogens that are quite different from each other the overall phase behavior of the system can be significantly modified from that of the pure compounds. The use of mixtures is standard in the LC industry for tuning the desired phase behavior. Phase separation in LC/polymer mixtures is a well-known process that can be used to produce polymer dispersed LC devices (PDLCs).[22] In that case, under controlled cooling conditions, micro-phase separation of the material into polymer-rich droplets in a nematic rich host phase is achieved with controllable droplet size and distribution.

At the isotropic to nematic phase transition in a homogeneous liquid crystal, domains of nematic ordering nucleate and grow as the material is cooled through the transition. At this point any dispersed NPs in the material will respond to the local order parameter and have been shown to preferentially locate in the shrinking isotropic domains. Such a particle sorting process can result in interesting pattern formation.[23,24] In general the inclusion of small colloidal particles in a liquid crystal phase will result in an elastic deformation of the director and a corresponding increase in the free energy density of the material. To reduce such deformation, particles may cluster or locate in areas of low molecular order such as at the center of topological defects. These effects play a key role in our mechanism for NP shell formation. As we will describe, liquid crystal phase separation of mesogen-functionalized QD rich droplets at the isotropic to nematic transition and their subsequent thermodynamic stabilization, leads to the formation of the well-defined vesicle-like structures.

This is not the first time spherical nanoparticle structures have been formed in soft matter systems and assembly can be achieved to a certain extent using a variety of different methods including evaporation[25,26] and other interfacial assembly mechanisms.[27] Progress was recently made using polymer-based methods to form NP-rich vesicle-like structures. However the resulting structures use much larger particles, producing assemblies more akin to colloidosomes,[28] or are much smaller (nanoscale), or softer (polymer embedded particles) with less well defined particle packing.[29,30] In particular, the structures we describe are very robust to high temperatures and mechanical deformation and can be produced in bulk without the need for microfluidic methods.

Our approach is based on the idea that a careful choice of anisotropic host phase and mesogenic surface ligands can provide an excellent route to self-assembled nanostructure stability and tunability. In this work, we use the isotropic to nematic phase transition to template micron-scale spherical nanoparticle constructs. The incorporation of a photo-cross-linkable functional group into the mesogenic ligand's framework provides a means of creating a covalently linked network after self-assembly of the NP-shell. Cross-linking further increases shell stability, opening up a wide variety of solution-processable uses in optically active coatings and inks or as stable vesicle-like structures for encapsulation applications.

Results

The mesogenic ligands investigated are shown in Fig. 1. All molecules contain a rigid aromatic core region surrounded by flexible domains at the termini, which gives the ligand the ability to interact with the host liquid crystal matrix to produce a uniform dispersion. The ligands investigated in this study are divided into two classes; the standard mesogenic (L1 and L2) and crosslinkable (L3 and L4) structures, both containing a varying length in the alkyl amine side-arm, which attaches the ligand to the particle surface. Synthesis of these molecules was carried out as previously reported[17] with detailed synthesis in the ESI.† These ligands exhibit liquid crystalline phases in their pure state with high clearing points above 100 °C – a contrast with the host phase (5CB (4-cyano-4′-pentylbiphenyl)), which exhibits the nematic to isotropic transition at 34 °C.

Ligands are exchanged on to the surface of CdSe quantum dots (5.2–6.2 nm, NN Labs Inc.) to form LC–QDs. These new particles are then dispersed into the common nematic liquid crystal, 5CB by wt%. Bath sonication for eight hours at 40 °C in the isotropic phase ensures an excellent initial dispersion, verified by fluorescence microscopy.

Once a homogenous suspension is obtained, nanoparticle shell formation is initiated by a fast cooling stage. As the composite material is cooled into the nematic phase by immediate transfer from a 40 °C heating block to a second temperature stage, at 30 °C, the system phase-separates into LC–QD rich droplets in an LC–QD poor (5CB rich) host phase. During this stage of the process, the functionalized QDs partition into shrinking isotropic domains mainly due to elastic forces.[23] Eventually a dense spherical wall of QDs is observed to form and no further shrinkage is observed (shell formation can be observed in ESI Videos 1 and 2†). As the isotropic domains, rich in LC–QDs, shrink, they gather nanoparticles, concentrating

them at the shrinking interface. This behaviour is expected if the timescale of droplet formation is faster than the timescale required for uniform Brownian particle dispersion within the droplet. At high concentration at the droplet inter-face, the particles interact and pack densely, forming the solid shell.

We have qualitatively observed that by varying initial QD concentration in the nematic host, shell size can be controlled. After formation, each shell contains QDs swept up from a local volume. At low overall LC–QD concentrations (~0.1 wt%), micron-sized droplets form, similar to those recently reported by our group[17] – in fact on close inspection these may be very small shells. Concentrations ranging from 0.1 to 0.5 wt% yield well defined shells as seen in Fig. 2. Higher concentrations produce a messier result with increasing amounts of QDs found outside of the shell. The formation process can be carried out on a microscope slide or alternately will produce a large number of shells when carried out in bulk (using a 1 ml Eppendorf tube). After formation, the shells can be pipetted out or centrifuged to concentrate at the bottom of the tube without noticeable damage or deformation.

Fluorescence microscopy can be used to track QD organization throughout the transition and therefore elucidate the shell formation process (Movie S1†). Fig. 2b and c show corresponding fluorescence and birefringence images of a few shells. In Fig. 2c the host nematic phase appears dark because the nematic director $\boldsymbol{n}$ is oriented parallel with one of the crossed polarizer directions (indicated by the white arrows). This image highlights the birefringence of the shell interior (an area depleted of fluorescent QDs) and the topological defects surrounding the shells. Colloidal particles with a radial ligand distribution producing either homeotropic or planar surface anchoring conditions create characteristic topological defects when surrounded by the nematic phase. Such defects can be visualized with optical microscopy, providing information on ligand organization at the particle surface. The presence of horizontal saturn ring defects around some shells in Fig. 2c implies that the outer ligands are aligned parallel to the shell surface, producing a planar surface anchoring condition. In addition bipolar-type defects are also observed as expected for this geometry.[31] In this image the surrounding 5CB material is aligned using a standard rubbed polyvinyl alcohol (PVA) alignment layer for optimal defect visualization. Detailed observations of a large number of shells revealed that they consistently appear to exhibit planar surface anchoring and defects representative of a vertical surface alignment were not seen. It will be very interesting in the future to look at how modification of the ligand structure can be used to vary ligand orientation on the shell surface.

Temperature and mechanical stability

Two different versions of the QD shells were tested for temperature stability, using ligands L1 and L2. In both cases we observed that shell structures were very robust to temperature change and appeared quite rigid when dispersed in the liquid crystal phase. On reheating the system to the liquid crystal isotropic point, no noticeable shape changes were observed in the shells despite significant flow of the surrounding liquid crystal. At the transition point, where isotropic domains began to nucleate in the host phase, the already formed shells moved into those domains and clustered. This observation is

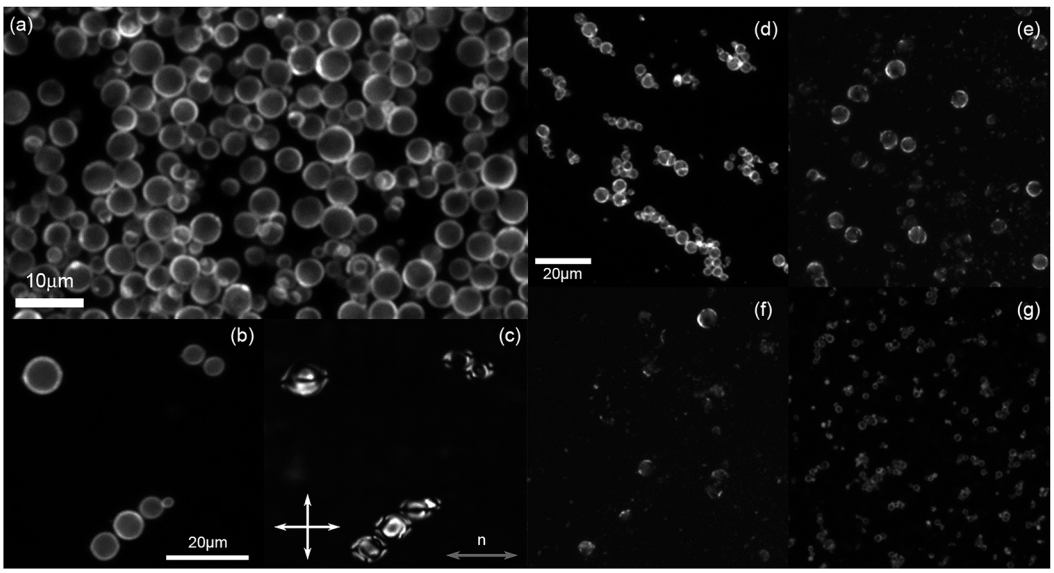

Fig. 2 (a) Fluorescence microscopy images of QD shells formed from 620 nm CdSe/ZnS QDs, functionalized with ligand L1 suspended in nematic liquid crystal at room temperature. (b) Fluorescence microscopy shows QD distribution for a few shells and (c) shows a polarized optical microscopy image of the same sample area. The polarizers are crossed as indicated by the white arrows and the material is oriented such that the nematic director, $\boldsymbol{n}$, is parallel to one of the polarizers as shown highlighting topological defects around the shells. A rubbed PVA alignment layer was used to provide planar alignment for this sample. In particular we can see 'saturn-ring' and 'bipolar' defects. QD shells prepared using ligand L2 are shown stable at room temperature (d), beginning to disperse at 115 °C (e), at 120 °C (f) and (g) at room temperature reformed after re-cooling.

consistent with our previous observations of nanoparticle aggregate formation at the same transition point.[23] The micron-scale size of these shells suggests that elastic forces dominate this process.

Once formed, the shells are very stable in 5CB. After heating above the liquid crystal isotropic point (34 °C) the shells for both tested ligands continued to maintain a rigid spherical structure on slow heating (1° min^{-1}). Observing the tumbling motion of some shells with surface imperfections in the melted (isotropic) 5CB helped us to come to this conclusion. In fact, no thermal shape fluctuations were observed at all up to more than 110 °C and the shells moved freely around the microscope slide without bursting, deforming or fusing with each other or the glass surface.

At high temperatures fragmentation was observed and the QDs re-dispersed into the surrounding material. Fig. 2 illustrates this process for ligand L2. In this case, when observed on a microscope slide, the shells started to break apart at 115 °C (Fig. 2e). Complete re-dispersion took place over a fairly broad temperature range (~10 °C). Interestingly we found that the process was somewhat reversible and after heating the material to a uniform state at 125 °C, the shells could subsequently be reformed by an additional rapid cooling step to produce smaller shell structures. We attribute the smaller size of these "secondary" shells to an imperfect re-dispersion. This would overall reduce the typical concentration in a given volume, therefore producing smaller shells. The observed shell 'melting' temperature for each ligand tested was far above the clearing point of pure 5CB and closer to that of the pure ligand. These observations demonstrate an important point – once formed, the elastic forces that govern the self-assembly process are no longer important for maintaining shell stability. Instead we propose that local interactions between ligand molecules in the shell provide the driving force for stabilization.

Structural characterization

To investigate this hypothesis further we carried out a detailed structural characterization of the system using small angle X-ray scattering (SAXS) and transmission electron microscopy (TEM).

As a comparison, SAXS and TEM on nanoparticle clusters in the nematic phase using ODA ligands indicate aggregates with a fractal-like, disordered structure. For the structures we present here, TEM confirmed the hollow vesicle-like shell morphology and on close inspection revealed the shell wall to be a dense, randomly packed assembly of the nanoparticles (Fig. 3a–c).

Nanoparticle packing in the QD–LC-ligand shells was quantified using SAXS, varying QD concentration and ligand type. The scattering patterns shown in Fig. 3 reveal an interesting result. The broad unoriented peak (A), at $q = 0.0616$ Å^{-1} represents a real-space distance of 10.20 nm and can be assumed to correspond to the average spacing between quantum dots in the shell wall. This number matches the expected separation of QDs shielded by bulky mesogenic ligands and is consistent with our previously reported interparticle separations in disordered aggregates of QDs functionalized with ligand L1.[17] Peak A is fairly broad, indicative of a relatively disordered particle packing and consistent with the TEM observations and calculated FFT (Fig. 3a–c).

QDs functionalized with ligand L2 bearing a shorter connecting arm, produced a slight shift in peak A (Fig. 3f). This new position corresponds to a QD spacing of 9.94 nm, compared to 10.20 nm for the longer connecting arm of ligand L1. This decrease in particle spacing is consistent with the shorter ligand–particle standoff distance as a result of the three carbon truncation in the amine containing chain, thus reducing the average particle separation within the shells.

A second interesting feature in the diffraction pattern is the sharp polycrystalline ring at position B, at 0.128 Å^{-1}, also visible as sharp spots on the CCD image (Fig. 3e). This peak is indicative of a relatively well-defined crystalline structure of length scale 4.9 nm. This *d*-spacing, while clearly too small to correspond to an inter-nanoparticle separation, matches the end-to-end dimensions of the ligand molecule rigid core quite well. From this result, and general observations of the mechanical rigidity of the shell walls, we conclude that this sharp peak originates from local ligand crystallization within the shell wall. We propose that as the LC–QDs are concentrated at the droplet interface during formation, they become stabilized by ligand–ligand interactions at a particular drop size. This droplet size in turn is dependent on the initial concentration of the composite.

Summarizing the above results and discussion, Fig. 4(a–e) shows several fluorescence microscopy snapshots of the formation process, clearly showing QD segregation, droplet formation and wall thickening. The isotropic to nematic phase transition templates QD assembly at the phase boundary. Two ESI movies (S1 and S2)† and Fig. 4f summarize the fast formation mechanism. Fig. 4g and h shows schematics of the shell structure. The shell walls consist of a densely packed assembly of functionalized particles, stabilized by ligand–ligand interactions. The surface of the shell structure adopts a planar surface-anchoring configuration as deduced from defect arrangements in the surrounding nematic phase.

Ligand cross-linking and shell extraction

Having confirmed that the relatively robust QD shells are stable to temperatures up to ~120 °C in the host LC material, it was then important to see if the shells could be removed from the host liquid crystal material and resuspended in different solvents. Achieving this step greatly broadens potential applications for the assemblies. The LC host material 5CB is a viscous fluid with distinct optical properties. Redispersing the assemblies in an organic solvent such as toluene allows them to be processed for use in a variety of coatings and solution-based formulations.

To achieve cross-linking, the shells were first formed as described previously, but using the UV cross-linkable ligands L3 and L4 which incorporate an electron poor-aryl azide in place of the distal benzoic acid moiety. In particular, we chose the tetrafluoro-arylazide group as it has been shown to act as an efficient nitrene precursor with a very high insertion efficiency.[32] Furthermore, this functional group has been successfully utilized to decorate carbon nanotubes,[33] photograft compounds

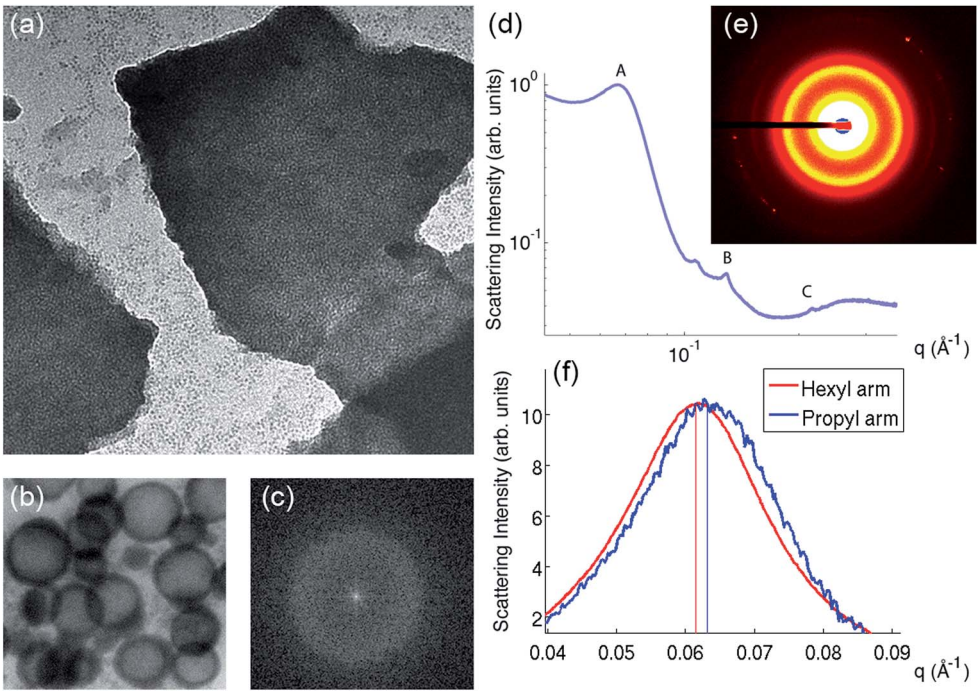

Fig. 3 Transmission electron microscopy images of QD shells. The main image (a) shows dense NP packing within fragments of a large shell after toluene extraction (image width, 1.4 μm). (b) A wider field image (width, 3.8 μm) of shells of the same composition in 5CB (c) FFT of a 0.67 μm wide area in the center of the large fragment. (d) X-ray scattering data for QD shells with ligand L1 in nematic liquid crystal radially integrated and (e) CCD scattering pattern corresponding to the data in (d). (f) Comparison of peak A for two different ligands L1 (hexyl arm) and L2 (propyl arm).

onto amorphous glasses[34] and affix fluorescent labels to proteins.[35]

To demonstrate that the shells could be extracted from the liquid crystal host and re-dispersed in a different solvent we formed shells in bulk cooling the host phase from isotropic to nematic as described earlier. The material was then exposed to a 6.4 mW cm^{-2} UV lamp (364 nm) for 1.5 h. Some shells were pipetted from the bulk after formation and diluted in a larger

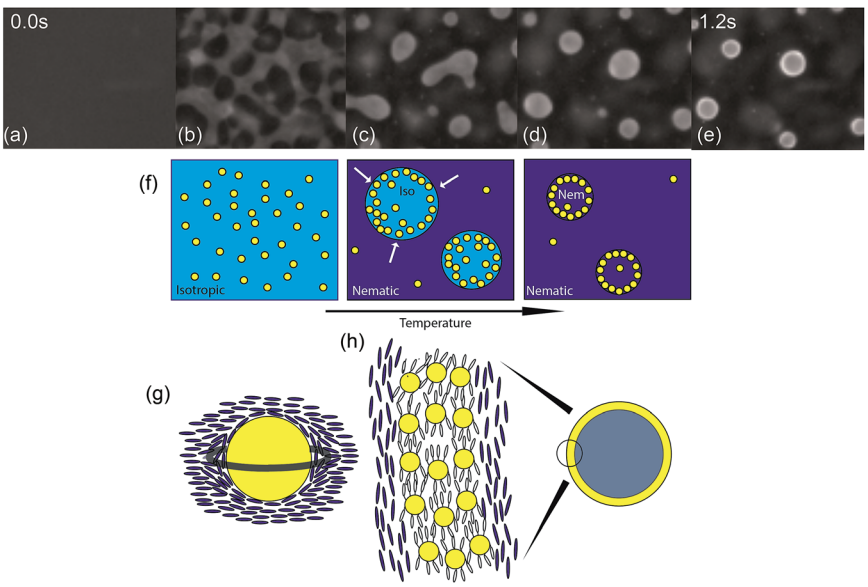

Fig. 4 (a–e) Snapshots from a high speed fluorescence video demonstrating the nanoparticle shell formation process by visualizing QD distribution over 1.2 s. Image width = 60 μm (ESI Video 1†). ESI Video 2† shows a wider field view demonstrating rapid bulk formation with an image width of 460 μm. Below in (f) cartoons represent the process. Ligand organization around the finished shells is confirmed by the presence of saturn-ring defects (g), observed experimentally using polarized optical microscopy (see Fig. 2c). (h) Proposed structure for the QD shell – QDs pack closely with a tactoidal ligand arrangement[18] to form the shell wall and LC ligands orient to create planar surface anchoring.

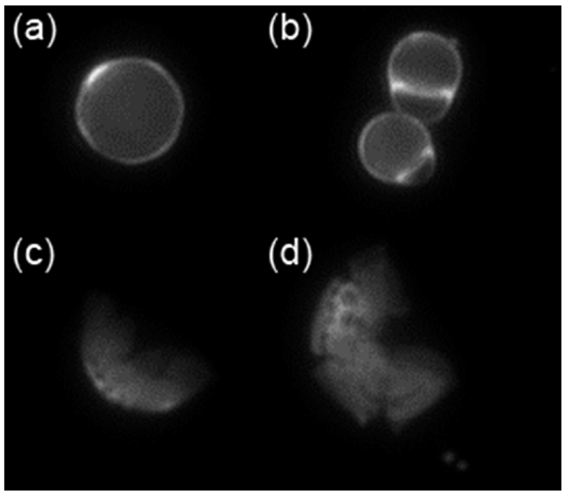

Fig. 5 Fluorescence microscopy images of cross-linked QD shells formed from ligand L3 (a) and (b) show examples of intact shells in toluene, (c) and (d) show examples of ruptured shells made of QDs functionalized with L4 after toluene evaporation.

volume of toluene, effectively removing the nematic phase. This toluene mixture was then placed on a microscope slide and the shells imaged *via* fluorescence microscopy as the toluene slowly evaporated. We observed that intact spherical shell structures were still present after the toluene dilution step (Fig. 5a and b), indicating that they are robust enough to be extracted for applications. After solvent evaporation, the dry shells tended to split, but still maintained their solid-wall structure (Fig. 5c and d), further demonstrating their structural integrity.

Conclusions

This paper presents a new methodology for the formation of self-assembled nanoparticle micro-shells. The structures are templated at the isotropic to nematic phase boundary in a liquid crystal host material using a process mediated by tunable mesogenic surface ligands.

Chemical control of shell size and structure is achieved by varying NP concentration and connecting ligand design. Since these parameters are independent of particle type, the process can be easily adapted for use with any appropriately sized NPs or combinations thereof, including mixtures of metallic, semiconducting and magnetic particles. This new method opens up a huge number of possibilities for the creation of non-planar 3D nano-assemblies, templated by the geometry of different liquid crystal phase transitions. and could be used to generate a new class of customizable capsules for photonics and condensed matter applications or bio-molecular encapsulation.

Acknowledgements

This work was supported in part by a grant from the nanoBIO node of the National Science Foundation (ECC-1227034), the Materials Research Laboratory (University of Illinois at Urbana-Champaign), and Professor Cathy Murphy's Laboratory (University of Illinois at Urbana-Champaign). The authors would also like to acknowledge generous funding from National Science Foundation grants DMR 0852791, DMR 1056860, and from the University of California, Merced Graduate and Research Council. Student funding (to B.H.C.) was provided by the NSF-COINS program (*via* UC Berkeley) under contract no. 0832819 and AR received additional funding from the UC President's Dissertation Year Fellowship. We would also like to thank Tayebeh Riahinasab for performing supplementary ligand characterization. Use of the Stanford Synchrotron Radiation Lightsource, SLAC National Accelerator Laboratory, is supported by the U.S. Department of Energy, Office of Science, Office of Basic Energy Sciences under Contract no. DE-AC02-76SF00515.

Notes and references

1 K. Overgaag, W. Evers, B. de Nijs, R. Koole, J. Meeldijk and D. Vanmaekelbergh, Binary Superlattices of PbSe and CdSe Nanocrystals, *J. Am. Chem. Soc.*, 2008, **130**, 7833–7835.
2 A. Tao, P. Sinsermsuksakul and P. Yang, Tunable plasmonic lattices of silver nanocrystals, *Nat. Nanotechnol.*, 2007, **2**, 435–440.
3 A. Claridge Shelley, A. W. Castleman, S. N. Khanna, C. B. Murray, A. Sen and P. S. Weiss, Cluster-Assembled Materials, *ACS Nano*, 2009, **3**, 244–255.
4 F. X. Redl, K.-S. Cho, C. B. Murray and S. O'Brien, Three-dimensional binary superlattices of magnetic nanocrystals and semiconductor quantum dots, *Nature*, 2003, **423**, 968–971.
5 S. Sun, C. B. Murray, D. Weller, L. Folks and A. Moser, Monodisperse FePt nanoparticles and ferromagnetic FePt nano-crystal superlattices, *Science*, 2000, **287**, 1989–1992.
6 A. Dong, J. Chen, P. M. Vora, J. M. Kikkawa and C. B. Murray, Binary nanocrystal superlattice membranes self-assembled at the liquid–air interface, *Nature*, 2010, **466**, 474–477.
7 J. M. Romo-Herrera, R. A. Alvarez-Puebla and L. M. Liz-Marzan, Controlled assembly of plasmonic colloidal nanoparticle clusters, *Nanoscale*, 2011, **3**, 1304–1315.
8 Y. Ofir, B. Samanta and V. M. Rotello, Polymer and biopolymer mediated self-assembly of gold nanoparticles, *Chem. Soc. Rev.*, 2008, **37**, 1814–1825.
9 W. Cheng, M. J. Campolongo, J. J. Cha, S. J. Tan, C. C. Umbach, D. A. Muller and D. Luo, Free-standing nanoparticle superlattice sheets controlled by DNA, *Nat. Mater.*, 2009, **8**, 519–525.
10 S. Srivastava, B. L. Frankamp and V. M. Rotello, Modulation of the Interparticle Spacing and Optical Behavior of Nanoparticle Ensembles using a Single Protein Spacer, *Chem. Mater.*, 2005, **17**, 487–490.
11 W. Shenton, S. A. Davis and S. Mann, Directed Self-Assembly of Nanoparticles into Macroscopic Materials Using Antibody–Antigen Recognition, *Adv. Mater.*, 1999, **11**, 449–452.
12 M. R. Bockstaller, Y. Lapetnikov, S. Margel and E. L. Thomas, Size-Selective Organization of Enthalpic Compatibilized

Nanocrystals in Ternary Block Copolymer/Particle Mixtures, *J. Am. Chem. Soc.*, 2003, **125**, 5276–5277.

13 H. Cui, Z. Chen, S. Zhong, K. L. Wooley and D. J. Pochan, Block Co-polymer Assembly *via* Kinetic Control, *Science*, 2007, **317**, 647–650.

14 J. He, Y. Liu, T. Babu, Z. Wei and Z. Nie, Self-Assembly of Inorganic Nanoparticle Vesicles and Tubules Driven by Tethered Linear Block Copolymers, *J. Am. Chem. Soc.*, 2012, **134**(28), 11342–11345.

15 J. Mirzael, M. Urbanski, H.-S. Kitzerow and T. Hegmann, Synthesis of Liquid Crystal Silane-Functionalized Gold Nanoparticles and Their Effects on the Optical and Electro-Optic Properties of a Structurally Related Nematic Liquid Crystal, *ChemPhysChem*, 2014, **15**(7), 1381–1394.

16 M. F. Prodanov, N. V. Pogorelove, A. P. Kryshtal, A. S. Klymchenko, Y. Mely, V. P. Semynozhenko, A. I. Krivoshey, Y. A. Reznikov, S. N. Yarmo-lenko, J. W. Goodby and V. V. Vashchenko, Thermodynamically Stable Dispersions of Quantum Dots in a Nematic Liquid Crystal, *Langmuir*, 2013, **29**, 9301–9309.

17 A. L. Rodarte, Z. S. Nuno, B. H. Cao, R. J. Pandolfi, M. Quint, S. Ghosh, J. Hein and L. S. Hirst, Tuning quantum dot organization in liquidcrystal for robust photonics applications, *ChemPhysChem*, 2014, **15**(7), 1413–1421.

18 M. Draper, I. M. Saez, S. J. Cowling, P. Gai, B. Heinrich, B. Donnio, D. Guillon and J. W. Goodby, Self-Assembly and Shape Morphology of Liquid Crystalline Gold Metamaterials, *Adv. Funct. Mater.*, 2011, **21**(7), 1260–1278.

19 X. B. Mang, X. B. Zeng, B. J. Tang, F. Liu, G. Ungar, R. B. Zhang, L. Cseh and G. H. Mehl, Control of Anisotropic Self-assembly of Gold Nanoparticles Coated with Mesogens, *J. Mater. Chem.*, 2012, **22**, 11101–11106.

20 W. Lewandowski, K. Jatczak, D. Pociecha and J. Mieczkowski, Control of Gold Nanoparticle Superlattice Properties *via* Mesogenic Ligand Architecture, *Langmuir*, 2013, **29**(10), 3404–3410.

21 M. Wojcik, W. Lewandowski, J. Matraszek, J. Mieczkowski, J. Borysiuk, D. Pociecha and E. Gorecka, Liquid–Crystalline Phases Made of Gold Nanoparticles, *Angew. Chem., Int. Ed.*, 2009, **48**(28), 5167–5169.

22 L. Boutellier and P. LeBarney, Polymer dispersed liquid crystals: preparation, operation and application, *Liq. Cryst.*, 1996, **21**(2), 157–174.

23 A. L. Rodarte, R. Pandolfi, S. Ghosh and L. S. Hirst, Quantum dot/liquid crystal composite materials: self-assembly driven by liquid crystal phase transition templating, *J. Mater. Chem. C*, 2013, **1**, 5527–5532.

24 J. Milette, S. J. Cowling, V. Toader, C. Lavigne, I. M. Saez, R. B. Lennox, J. W. Goodby and L. Reven, Reversible long-range network formation in gold nanoparticle – nematic liquid crystal composites, *Soft Matter*, 2012, **8**(1), 173–179.

25 J. B. Miller, A. C. P. Usselman, R. J. Anthony, U. R. Kortshagen, A. J. Wagner, A. R. Denton and E. K. Hobbie, Phase separation and the coffee-ring effect in polymer-nanocrystal mixtures, *Soft Matter*, 2014, **10**, 1665–1675.

26 H. Wu, L. X. Chen, X. Q. Zeng, T. H. Ren and W. H. Briscoe, Self-assembly in an evaporating nanofluid droplet: rapid transformation of nanorods into 3D fibre network structures, *Soft Matter*, 2014, **10**, 5243–5248.

27 M. Ali, S. K. Pal, H. Rahaman and S. K. Ghosh, Interfacial assembly of ZnO quantum dots into giant supramolecular architectures, *Soft Matter*, 2014, **10**, 2767–2774.

28 J. S. Sander and A. R. Studart, Monodisperse functional colloido-somes with tailored nanoparticle shells, *Langmuir*, 2011, **27**, 3301–3307.

29 R. J. Hickey, X. Meng, P. Zhang and S.-J. Park, Low-dimensional nanoparticle clustering in polymer micelles and their transverse relaxivity rates, *ACS Nano*, 2013, **7**(7), 5824–5833.

30 M. Kanahara, H. Yabu and M. Shimomura, Fabrication of gold nanoparticle/polymer composite particles with raspberry, core–shell and amorphous morphologies at room temperature *via* electrostatic interactions and diffusion, *Soft Matter*, 2013, **10**, 275–280.

31 P. S. Drzaic, Polymer dispersed nematic liquid crystal for large area displays and light valves, *J. Appl. Phys.*, 1986, **60**(6), 2142–2148.

32 S. X. Cai, J. C. Nabity, M. N. Wybourne and J. F. W. Keana, Bis(perfluorophenyl) azides – efficient cross-linking agents for deep-UV and electron-beam lithography, *Chem. Mater.*, 1990, **2**, 631–633.

33 S. J. Pastine, D. Okawa, B. Kessler, M. Rolandi, M. Llorente, A. Zettl and J. M. J. A. Fréchet, *J. Am. Chem. Soc.*, 2008, **130**, 4238–4239.

34 J. Amalric, C. Hammaecher, E. Goormaghtigh and J. Marchand-Brynaert, Surface Photografting of Arylazide Derivatives on Chalco-genide Glasses, *J. Non-Cryst. Solids*, 2014, **387**, 148–154.

35 D. Verga, F. Hamon, F. Poyer, S. Bombard and M.-P. Teulade-Fichou, Photo-Cross-Linking Probes for Trapping G-Quadruplex DNA, *Angew. Chem., Int. Ed.*, 2013, **53**, 994–998.